

# Classification and Staging of Chronic Liver Disease From Multimodal Data

Ricardo T. Ribeiro\*, Rui Tato Marinho, and J. Miguel Sanches, *Senior Member, IEEE*

**Abstract**—Chronic liver disease (CLD) is most of the time an asymptomatic, progressive, and ultimately potentially fatal disease. In this study, an automatic hierarchical procedure to stage CLD using ultrasound images, laboratory tests, and clinical records are described. The first stage of the proposed method, called *clinical based classifier* (CBC), discriminates healthy from pathologic conditions. When nonhealthy conditions are detected, the method refines the results in three exclusive pathologies in a hierarchical basis: 1) chronic hepatitis; 2) compensated cirrhosis; and 3) decompensated cirrhosis. The features used as well as the classifiers (Bayes, Parzen, support vector machine, and  $k$ -nearest neighbor) are optimally selected for each stage. A large multimodal feature database was specifically built for this study containing 30 chronic hepatitis cases, 34 compensated cirrhosis cases, and 36 decompensated cirrhosis cases, all validated after histopathologic analysis by liver biopsy. The CBC classification scheme outperformed the non-hierarchical one against all scheme, achieving an overall accuracy of 98.67% for the normal detector, 87.45% for the chronic hepatitis detector, and 95.71% for the cirrhosis detector.

**Index Terms**—Chronic liver disease (CLD), cirrhosis, classification, ultrasound-based textural features.

## I. INTRODUCTION

**C**HRONIC liver disease (CLD) is a significant cause of morbidity and mortality in developed countries and is commonly caused by viral hepatitis and alcohol abuse [1]–[3]. The initial stages of CLD are usually asymptomatic such as *hepatitis* or *steatosis*. *Hepatitis*, a liver inflammation, may lead to cell damage and/or destruction [1]. Repeated cycles of inflammation (fibrosis), necrosis, and hepatocellular regeneration contribute to the development of liver *cirrhosis* [2], [3]. This is a

potentially fatal process with a high probability of *hepatocellular carcinoma* development [2].

It is possible to distinguish two phases in liver *cirrhosis*: a stable form, called *compensated cirrhosis*, that is frequently asymptomatic and unsuspected; and a more dangerous form related to liver failure, called *decompensated cirrhosis* [4].

Liver biopsy is the gold standard for the evaluation and staging of CLD. However, its invasive nature prevents its generalized usage in the first stages of the diagnosis process. By this, noninvasive methods for CLD diagnosis with similar accuracy [5], [6] have been proposed in the literature.

Typical noninvasive methods [7], [8] are the APRI (*aspartate aminotransferase* (AST)/platelet ratio index), the Forns index (based on age, platelets, *gamma-glutamyl transferase* (gGT) and cholesterol), the *FibroTest* (FT), *FibroMeter* (FM), *Hepascore* (HS), and new ultrasound-based technologies, such as *transient elastography* (TE).

FT is proprietary commercial test [9] available in many, but not all, clinical institutions. The authors of [9] reported a sensitivity of about 75% and a specificity of 85%. FM combines hyaluronate, prothrombin time, platelets, AST, alpha2 macroglobulin, urea, and age [10]. The FM formula is adjusted based on the cause of liver disease [11], and it has been shown to be an accurate predictor for chronic viral hepatitis [9]. HS combines bilirubin, gGT, hyaluronic acid, alpha2 macroglobulin, age, and gender [11]. Isolated usage of APRI index does not provide information equal to the one provided by liver biopsy in most patients with CLD [9]. TE induces an elastic shear wave that is detected by pulse-echo US as the wave propagates through the organ and estimates liver stiffness. A metaanalysis study stated promising results for the detection of cirrhosis but revealed great variability in the detection of severe fibrosis [9].

The combination of these markers in a sequential basis performs better than each marker alone. The *sequential algorithm for fibrosis evaluation* (SAFE) biopsy is a decision tree classifier trained in *hepatitis C virus* (HCV) patients [12], [13]. The SAFE algorithm integrates APRI test and FT, and for inconclusive results biopsy is suggested. The authors of [8] propose the combination of TE and FT as first line assessment of fibrosis and when both indicators do not agree, biopsy is used.

These methods, however, are not reliable alternatives to biopsy, because they present several limitations and they do not meet consensus in the medical literature.

In this study, inspired by the clinical practice, we propose a classification strategy, called *the clinical-based classifier* (CBC), for the assessment of CLD based on a multimodal feature approach, extracted from *ultrasound* (US) images, laboratory tests, and clinical data. We also evaluate the influence of

Manuscript received March 14, 2012; revised June 19, 2012, September 12, 2012, November 7, 2012, and November 24, 2012; accepted December 1, 2012. Date of publication December 19, 2012; date of current version April 15, 2013. This work was supported by the Fundação para a Ciência e a Tecnologia (FCT) under Projects PEst-OE/EEI/LA0009/2011 and Project PTDC/SAU-BEB/104948/2008. Asterisk indicates corresponding author.

\*R. T. Ribeiro is with the Institute for Systems and Robotics, the Escola Superior de Tecnologia da Saúde de Lisboa, and the Bioengineering Department, Instituto Superior Técnico, Technical University of Lisbon, Lisbon 1990-096, Portugal (e-mail: ricardo.ribeiro@estes.ipl.pt).

R. T. Marinho is with the Liver Unit, Department of Gastroenterology and Hepatology, Hospital de Santa Maria, Medical School of Lisbon, Lisbon 1990-096, Portugal (e-mail: rui.marinho@mail.telepac.pt).

J. M. Sanches is with the Institute for Systems and Robotics and the Bioengineering Department, Instituto Superior Técnico/Technical University of Lisbon, Lisbon 1990-096, Portugal (e-mail: jmsr@ist.utl.pt).

Color versions of one or more of the figures in this paper are available online at <http://ieeexplore.ieee.org>.

Digital Object Identifier 10.1109/TBME.2012.2235438

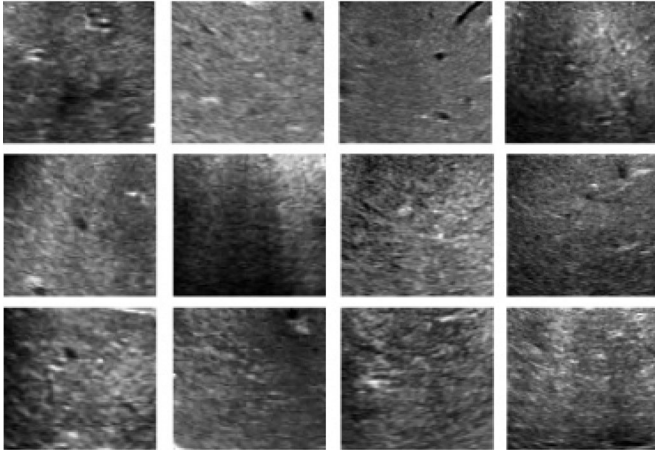


Fig. 1. US liver images variability in different CLD stages. Normal liver samples are represented in the first column, the second column presents samples from chronic hepatitis, and compensated and decompensated cirrhosis appear in the third and fourth column, respectively.

US-based features in the classification of CLD, comparing with the classification based on laboratory and clinical features.

It has been shown that US data, together with laboratory and clinical information, are useful in the characterization of CLD. Additionally, US scanners are available in almost all medical and clinical facilities and its noninvasive and nonionizing nature makes it a very appealing technology for widespread CLD diagnosis and follow-up protocols. In [1], it is shown that echogenicity, texture analysis, and surface morphology of the liver parenchyma are effective US features to stage CLD. Echogenicity is related to the echo gray level of the US image [14]. On the other hand, it is expected that textural analysis of the liver parenchyma contains information about fibrotic development, since tissue acoustic properties change [15].

Normal liver parenchyma appears homogeneous in US images, interrupted by normal blood vessels, bile ducts, and ligaments [14], [16]. Repeatedly, hepatic inflammation, described in chronic hepatitis and compensated cirrhosis, may lead to a coarse heterogeneous parenchyma [15]–[18], or maintain a normal appearance [14]–[16], with increased echogenicity. Decompensated cirrhosis is characterized by a coarse heterogeneous parenchyma with increased echogenicity and irregular contour [14]–[19].

The visual variability of US images in different stages of CLD, displayed in Fig. 1, justify the need of objective methods in feature extraction and classification, based on a *computer assisted diagnosis* (CAD) framework. Several studies use objective features extracted from US images and propose classification procedures to assess CLD [20]–[28]. This topic will be discussed in detail in Section II.

The key idea behind CBC is that the discriminative power of each classifier can be greatly improved if the disease’s natural evolution is taken into account. The CBC stages are optimized from a feature and classifier point of view, in order to select the best combination that leads, at each stage, to the higher accuracy.

The remainder of this paper is organized as follows. Section II introduces the study design and explains the

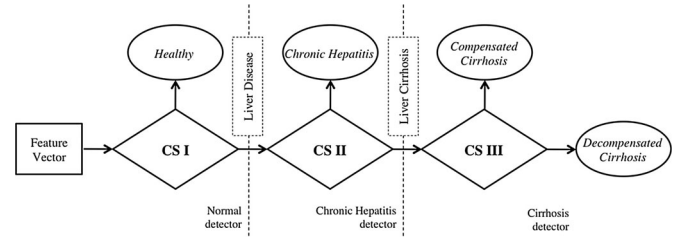


Fig. 2. CBC decomposition strategy design for CLD classification.

procedures of feature extraction and selection, as well as the classifiers and the dataset used in this study. In Section III, the results are presented and in Section IV their discussion are explored. Section V concludes this paper.

## II. METHODS

The CBC aims to discriminate normal and three main pathologies in the scope of CLD: 1) *chronic hepatitis* (CH); 2) *compensated cirrhosis* (CC); and 3) *decompensated cirrhosis* (DC). In clinical practice, the diagnosis of these pathologies is normally based on several sources of medical data such as US images, laboratory analysis, and clinical indicators recommended by well established and accepted medical guidelines [4]. The diagnosis, however, is obtained by integrating all the information with a subjective criteria and experience of the medical doctor.

The CBC is a hierarchical strategy, which mimics the hierarchical approach of *differential diagnosis* followed in clinical practice, to stage CLD. CBC is a more informative classification strategy that combines clinical, serologic, and histologic features [3]. This strategy has replaced CLD staging based only on the degree of hepatic fibrosis, as suggested in [21], [24], [29]–[31].

Instead of a *one against all* (OAA) strategy using a multiclass classifier [32], e.g., *k-nearest neighbor* (kNN), *Bayes*, *Parzen*, or *support vector machine* (SVM), the hierarchical approach, represented in Fig. 2, is used. In this strategy, several partial binary decisions are taken according to the disease natural evolution. The architecture of CBC is based on the transition rate between CLD stages and live expectancy. The transition from CH to CC and CC to DC occurs at a rate of 1–5% and 5–7% per year, respectively [33], [34]. The transition rate from CC to death and DC to death occurs at a rate of 3.4% and 57% per year, respectively [33].

The CBC’s first classification step (CS I) discriminates *healthy* from *pathologic* livers. If a liver is classified as *pathologic* in the first step, discrimination of CH and *cirrhosis* (CS II) is attempted. In the last step (CS III), CC and DC are discriminated. The DC class is assumed to be the end stage of CLD before *hepatocellular carcinoma* or death.

The design of the CBC approach is composed by three components: 1) features computation from multimodal sources; 2) design and training of a specific suitable classification strategy that takes into account the CLD specificities; and 3) diagnosis and validation of the method. For each CS, CBC is optimized at two levels (see Fig. 2): 1) feature selection and 2) classifier type and parametrization tuning.

Four types of classifiers, kNN, *Bayes*, *Parzen*, or SVM [32], are tested at each CS. The performance of each classifier, at each CS, is evaluated by means of *leave-one-out cross validation* (LOOCV) method. This method is useful in cases with small amount of available data, as normally observed in medical problems. Under LOOCV, the available data ( $N$ ) is divided into  $N$  disjoint sets;  $N$  models are trained, each on a different combination of  $N - 1$  partitions and tested on the remaining partition [35].

In each CS, the feature selection procedure is based on the stepwise regression analysis method [36] (criterion to add:  $p < 0.05$ ; to remove:  $p > 0.1$ ). To evaluate the redundancy between the selected features, we also calculate their *mutual correlations* (MC) [32]. The features selected in the preceding method were only retained if they produced an MC value lower than a threshold, set at 0.4.

The classifier selection is performed with an ROC analysis by means of *Youden's index* ( $J$ ) [32], where the *sensitivity* (sens) and the *specificity* (spec), in an LOOCV basis, are jointly maximized

$$\{\hat{k}, \hat{\theta}, \hat{\mathbf{f}}\} = \arg \max_{k, \theta(k), \mathbf{f}(k)} J(k, \theta(k), \mathbf{f}(k)) \quad (1)$$

where  $k$  is a classifier from the tested set of classifiers,  $\mathcal{K} = \{\text{kNN}, \text{Bayes}, \text{Parzen}, \text{SVM}\}$ ,  $\theta(k)$  are the parameters of the corresponding classifier, and  $\mathbf{f}(k)$  are the selected features for each classifier. Youden's index is defined as follows:

$$J(k, \theta(k), \mathbf{f}(k)) = \text{sens}(k, \theta(k), \mathbf{f}(k)) + \text{spec}(k, \theta(k), \mathbf{f}(k)) - 1. \quad (2)$$

The kNN classifier classifies a test sample according to the majority of its neighbors in the feature space by using the *minimum Euclidean distance* criterion [37], [38].

The *Bayes* classifier assumes that the vector of features are multivariate normal distributed [21], [24] with different means,  $\{\mu_1, \mu_2\}$  and covariance matrices,  $\{\Sigma_1, \Sigma_2\}$ . The corresponding quadratic discriminant function

$$g_\tau(\mathbf{x}) = -\frac{1}{2}(\mathbf{x} - \mu_\tau)^T \Sigma_\tau (\mathbf{x} - \mu_\tau) - \frac{1}{2} \log |\Sigma_\tau| + \log P(w_\tau) \quad (3)$$

with  $\tau \in \{1, 2\}$  is used in the classification of a given feature vector  $\hat{\mathbf{x}}$  according to

$$\begin{cases} 1 & \text{if } g_1(\hat{\mathbf{x}}) > g_2(\hat{\mathbf{x}}) \\ 2 & \text{otherwise.} \end{cases} \quad (4)$$

The *Parzen* classifier is very similar to the Bayes one but it does not assume a Gaussian distribution of the data. Instead, estimates the distribution density of the samples that constitute each class by summing the distance-weighted contributions of each sample in a class and classify a test sample by the label corresponding to the maximum posterior [32].

The SVM classifier aims at finding a decision plane that has a maximum distance (margin) from the nearest training pattern [21], [38]. This is performed by mapping the feature vector in a higher-dimensional space. In this new space the SVM finds a hyperplane to separate the two classes with a decision

boundary set by support vectors [21], [38]. The computationally intensive mapping process can be reduced with an appropriate kernel function. In this paper, the *polynomial* kernel is used.

The CBC performance is assessed by comparing at each classification step with the common OAA binary classifier, using one-way analysis of variance (ANOVA) with  $p < 0.01$ . In OAA, the classification problem is decomposed in several binary classification procedures, each per class.

### A. Features

The features extracted from multimodal sources are some of the most discriminative ones for diagnosis, as described in the following sections.

*Ultrasound Features:* Some specific features can be natural candidates to be used in the feature selection procedure [20]–[28], such as:

*Co-Occurrence:* The elements of the *co-occurrence* tensor,  $\mathbf{Co} = \{c_{i,j}(\Delta_l, \Delta_c)\}$ , describe the gray level spatial interrelationship in the image [39]. More precisely, element  $c_{i,j}(\Delta_l, \Delta_c)$  represents the joint probability of the pixel intensities  $i$  and  $j$  in the relative spatial position of  $(\Delta_l, \Delta_c)$  [39] and can be computed as follows:

$$c_{i,j}(\Delta_l, \Delta_c) = \sum_{l=1}^N \sum_{c=1}^M \begin{cases} 1 & \text{if } (\eta_{l,c} = i) \wedge (\eta_{l+\Delta_l, c+\Delta_c} = j) \\ 0 & \text{otherwise.} \end{cases} \quad (5)$$

For a pixel distance of 6, we have four angular  $[0^\circ, 45^\circ, 90^\circ, 135^\circ]$  *co-occurrence* tensors for  $(\Delta_l, \Delta_c) \in \{(0, 6), (-6, 6), (-6, 0), (-6, -6)\}$ , where we calculate the most commonly statistical features, based on [40], namely contrast, correlation, energy, and homogeneity.

*Wavelet Transform:* The *Wavelet Transform* (WT) provides multiscale features from the US images. The decomposition is performed according to a sequence of low pass ( $G$ ) and high-pass, ( $H$ ), filtering operations followed by down-sampling the results,  $\downarrow 2$ . This method generates a pyramidal representation of the original image with decreasing resolution comprising a lower resolution low-pass component (approximation component) (LL), and three high-pass components (detailed components) along the horizontal (HL), vertical (LH), and diagonal directions (HH). An example of a multiscale WT analysis using a US liver image is provided in Fig. 3. High-pass components ( $H$ ) contain image detailed information at different resolution scales along three directions, while low-pass versions ( $L$ ) contain the approximation component.

Liver tissue characterization based on WT multiresolution analysis has been performed in several works [21]–[24]. This approach is effective in the morphological characterization of the image from the approximation fields and at the same time in a textural characterization at several resolution scales from the detailed fields. In the present study, a second-order decomposition with Haar wavelet is used. For each subimage ( $HL_{1,2}$ ,  $LH_{1,2}$ , and  $HH_{1,2}$ ), the coefficients of the first-order 2-D autoregressive model are computed,  $\{a_{1,1}, a_{1,0}, a_{0,1}\}$ , as well as the energy and the mean.

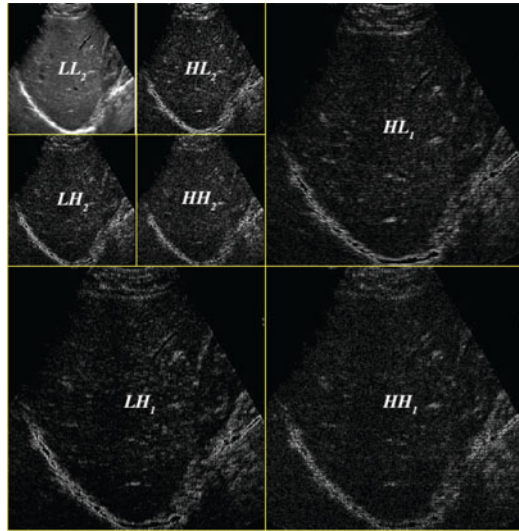


Fig. 3. Wavelet pyramidal decomposition example from a US liver image.

*Autoregressive Model (AR):* The AR model approach has been used for a long time with success in several applications of engineering where identification and characterization of systems and processes are needed [41]. In the canonical definition of a 1-D  $p$ -order AR model each sample is modeled as a linear combination of the previous  $p$  samples with unknown coefficients,  $a_k$  [27]

$$x(n) = \sum_{i=1}^p a_i x(n-i) + r(n) \quad (6)$$

where the residue signal  $r(n)$  is assumed to be white and zero mean normal distributed. For image applications the following 2-D formulation of the  $(p, q)$ -order AR model is used [28]

$$x(n, m) = \sum_{i=0}^p \sum_{j=0}^q a_{ij} x(n-i, m-j) + r(n, m) \quad (7)$$

where  $x(n, m)$  is the  $n, m$ th pixel of the image and  $a_{0,0} = 0$ .

There are many algorithms to compute AR parameters: Levinson Burg, least-squares, gradient based, lattice filter, and Kalman filter [42]. In this study, we use the most popular, the least-squares algorithm [28].

The order of the model  $(p, q)$  controls the error associated with the AR signal approximation [26]. Small orders ignore the main and long-term statistical properties of the original signal while larger ones may lead to overfitting effects [25], [26]. Therefore, selecting the order of the model is a key problem and there are several methods to do it [25]–[28]. Here, the first-order model was adopted because it was confirmed by [43] that in this scope it leads to the minimum error probability.

*Laboratory and Clinical Features:* Besides image-based features, several clinical data and laboratory tests are useful for evaluating and managing patients with hepatic dysfunction. These features are selected according to their purported clinical and pathophysiological role in CLD [33]. The clinical and pathophysiological characteristics of CLD can be grouped in hepatic insufficiency, portal hypertension, hyperdynamic cir-

ulation, liver inflammation, necrosis and fibrosis, as well as etiologic factors [33], [34], [44].

Hepatic insufficiency is suggested by the Child–Pugh score, albumin, total bilirubin, prothrombin time expressed as *international normalized ratio* (INR) [33], and portosystemic encephalopathy [45]. Portal hypertension is usually accessed by the presence of ascites, esophageal varices, and *gastrointestinal* (GI) bleeding. Creatinine and sodium are variables used for the study of hyperdynamic circulation [33]. Liver inflammation, necrosis, fibrosis, and histology can be evaluated based on AST, gGT, *lactate dehydrogenase* (LDH), and *alanine transaminase* (ALT) [10], [33].

Laboratory changes reveal, particularly, liver dysfunctions in CLD patients. Changes in AST and ALT reveal leakage from damaged hepatocytes; gGT and bilirubin are related to cholestasis and decreased hepatocyte and renal excretory function; albumin and INR report a decrease in hepatic production; and sodium imbalance reveals an inability to excrete free water via the kidneys [5]. Marked increase of LDH is found in patients with neoplasms with hepatic involvement, but is considered to be an insensitive index for hepatocellular injury [34]. Hyperglycemia is a comorbidity in patients with cirrhosis [33].

In a patient with CLD, relevant clinical characteristics are recorded, such as age, gender, etiology of CLD, CHILD, and clinical complications. CLD can have different etiologies, such as viral hepatitis (B, C, and D), alcohol, metabolic, disturbed immunity, toxins, therapeutic agents, and others [34]. *Disease cause* feature reports to CLD etiology and, in this study, patients were classified as follows: 1) no disease; 2) alcohol; 3) hepatitis B virus (HBV); 4) hepatitis C virus (HCV); 5) alcohol and HBV; 6) alcohol and HCV; and 7) other cause. The Child–Pugh score is a prognostic model used to predict mortality in cirrhosis and it is by far the most used in clinical practice and clinical research [33]. It uses five features: ascites, encephalopathy, prothrombin time, and serum levels of bilirubin and albumin [46]. Patients were classified with value 1 (class A), 2 (class B), or 3 (class C) in relation to best (A), moderate (B), or worse (C) prognosis [46].

Clinical complications, such as ascites, GI bleeding, encephalopathy, infection, and tumor, were clinically assessed according to their presence or absence. Changes in any of these clinical complications can mark the transition between CLD stages (CH to CC or CC to DC). Ascites is a fluid accumulation in the peritoneal cavity and its presence reveals clinically significant portal hypertension. GI bleeding from varices or mucosal congestion was defined by the presence of one of the following historical features: hematemesis, melena, hematochezia, or any combination of the above. GI bleeding can also precipitate hepatic encephalopathy. The presence of hepatic encephalopathy was made according to [47] after exclusion of intracranial lesions, metabolic, traumatic disorders, or drug intoxication. The presence of infections, particularly bacterial infections, is frequent and exacerbates hepatic dysfunction, encephalopathy, and portal hypertension [5]. The same behavior is observed when tumors are detected. The development of hepatocellular carcinoma may accelerate the course of the disease at any stage [33].

In [45], it is demonstrated that HCV chronic patients, with no decompensation episode, have a slow evolution to

cirrhosis. Esophageal varices, INR, gGT, bilirubin, and albumin were associated with an increased risk of clinical decompensation. By multivariate analysis, only esophageal varices and bilirubin were associated with increased risk of decompensation [45]. Several fibrosis indices and models have been developed using routine laboratory tests. Eighty-seven studies propose models to predict hepatic fibrosis in CH patients based on laboratory serum tests [48]. Using logistic regression, [49] identified platelet count, spider nevi, AST, and male gender as independent predictors of cirrhosis. APRI, the Forns Index, and the FT model (described in Section I) are also based on common laboratory tests [48]. Patients with alcoholic hepatitis demonstrate a wide range of clinical features [19]. Alcoholic cirrhosis range from asymptomatic to decompensated liver function with ascites, variceal hemorrhage, and encephalopathy. These patients have higher AST and ALT levels, hypoalbuminemia, hyperbilirubinemia, and prolonged prothrombin time [19].

A total of 68 features were extracted for each patient, 47 from the US image (first-order statistics, co-occurrence matrix, Haar wavelet decomposition, first order 2-D AR model coefficients), 11 from the laboratory tests (bilirubin, INR, albumin, creatinine, AST, ALT, gGT, glycemia, sodium, urea, and LDH) and 10 from clinical data (disease cause, tumor, ascites, encephalopathy, gastro-intestinal bleeding, infection, alcoholic habits, Child-Pugh score, age, and gender).

All features were available in each CS and no *a priori* selection was performed. The feature selection procedure, using stepwise regression with the MC criterion, produced an optimal subset of five features for CS I, six features for CS II, and ten features for CS III, as listed in Table II. This topic is further discussed in Section III.

### B. Dataset

A new dataset with liver information, medically validated, was built. A total of 100 patients with CLD, registered at the Liver Unity, Gastroenterology Department, of the Santa Maria Hospital in Lisbon, Portugal, were enrolled in the study. Patients were selected with known diagnosis according to the results from liver biopsy. Patients were excluded if they presented other liver disease or underwent treatment within the previous six months.

Based on CLD staging, 30 patients were diagnosed with CH, 34 diagnosed with CC, and 36 with DC. CLD was caused by virus infection in 39 patients (HBV = 11 and HCV = 28), by alcohol in 32 patients, combination of both in 14 and by other causes ( $n = 15$ ). A control group of 48 volunteers was set as the *Normal* class, where the inclusion criterion was to not have any known liver disease.

For each sample of the database ( $n = 148$ ) laboratory tests, clinical history and US images were collected in the same day. A total of 148 US liver images, from 148 patients, were involved in the experiments. Laboratory tests were performed in the referred hospital, with the following reference to normal values: bilirubin ( $<1.0$  mg/dL); albumin (3.7–5.8 g/dL); creatinine (0.5–1.1 mg/dL); AST (0–34 U/L); ALT (10–49 U/L); gGT ( $<38$  U/L); glycemia (70–110 mg/dL); sodium (135–145 mmol/L); urea (10–50 mg/dL); and LDH (208–378 U/L).

The criteria used for the assessment of the clinical features were similar to [45]. Ascites was diagnosed via clinical examination and/or US and encephalopathy is detected according to the usual clinical parameters. GI bleeding is positive if hematemesis and/or melena is observed and whenever possible, confirmed by endoscopy. Tumor and infections are assessed via specific biochemical markers.

This study was approved by the Ethics Committee of the referred hospital and an informed consent was obtained in accordance with the declaration of Helsinki principles.

The US liver protocol used in the hospital was adopted. For sake of reproducibility, consistency and diagnosis accuracy, we incorporate in this protocol the procedures proposed in [37]. Three main concerns were taken into account: 1) US scanner parameters; 2) patient position and cross-section selection; and 3) ROI selection.

The same US scanner (Philips CX50, Amsterdam, the Netherlands) was used for all acquisitions tuned with the same preset configuration, the commonest one used in clinical practice. A broadband curved array transducer (Philips C5-1, Amsterdam, the Netherlands) was used in all acquisitions with a central frequency of 3.5 MHz, an image depth of 150 mm and two focal zones were set at the central portion of the image (75 mm). The dynamic range is 75 dB, the depth gain compensation was set to its central position and the default grayscale colormap was used. A fixed set of anatomical landmarks on the right liver lobe are used in all acquisitions to capture equivalent liver cross sections. Patients were in supine position, comfortably installed and gently breathing to avoid movements.

Images were stored in DICOM format, 3 pixel/mm and 8 bit/pixel resolution. A ROI, of approximately  $128 \times 128$  pixels ( $45.7 \times 45.7$  mm) extracted by the operator from each image along the medial axis at a mean depth of 53 mm, should be representative of the liver parenchyma, free of major blood vessels and liver ligaments. It should also be as superficial as possible, to avoid US beam distortions [24], [37]. These requirements often prevent the ROI extraction from the ideal location, the focal zone.

## III. RESULTS

In this section, the results from real data, described in Section II-B, are presented to validate the proposed CBC method. All results were obtained with the MATLAB toolbox for pattern recognition, PRTools 4.1 [50].

For each CS, one out of four classifiers, kNN, *Parzen*, *Bayes*, and SVM, is selected according to the optimality criterion of minimum classification error. Different parameterizations of each classifier are tested. For kNN classifier, nine different neighborhood configurations were tested, corresponding to  $k = 1, \dots, 9$ . The SVM polynomial kernel was trained with the cost ( $c$ ) ranging  $c = 1, 10, 100, 500$ , and degree ( $d$ ),  $d = 1, 2, 3, 4, 5$ . Only the best results ( $c = 1$ ) are presented.

*CBC Strategy Versus OAA Strategy:* To validate the CBC strategy, a comparison with the OAA strategy was performed, using the same experimental conditions.

The binary combination in the *normal* detector (CS I) is equal in both decomposition strategies and the results are resumed in

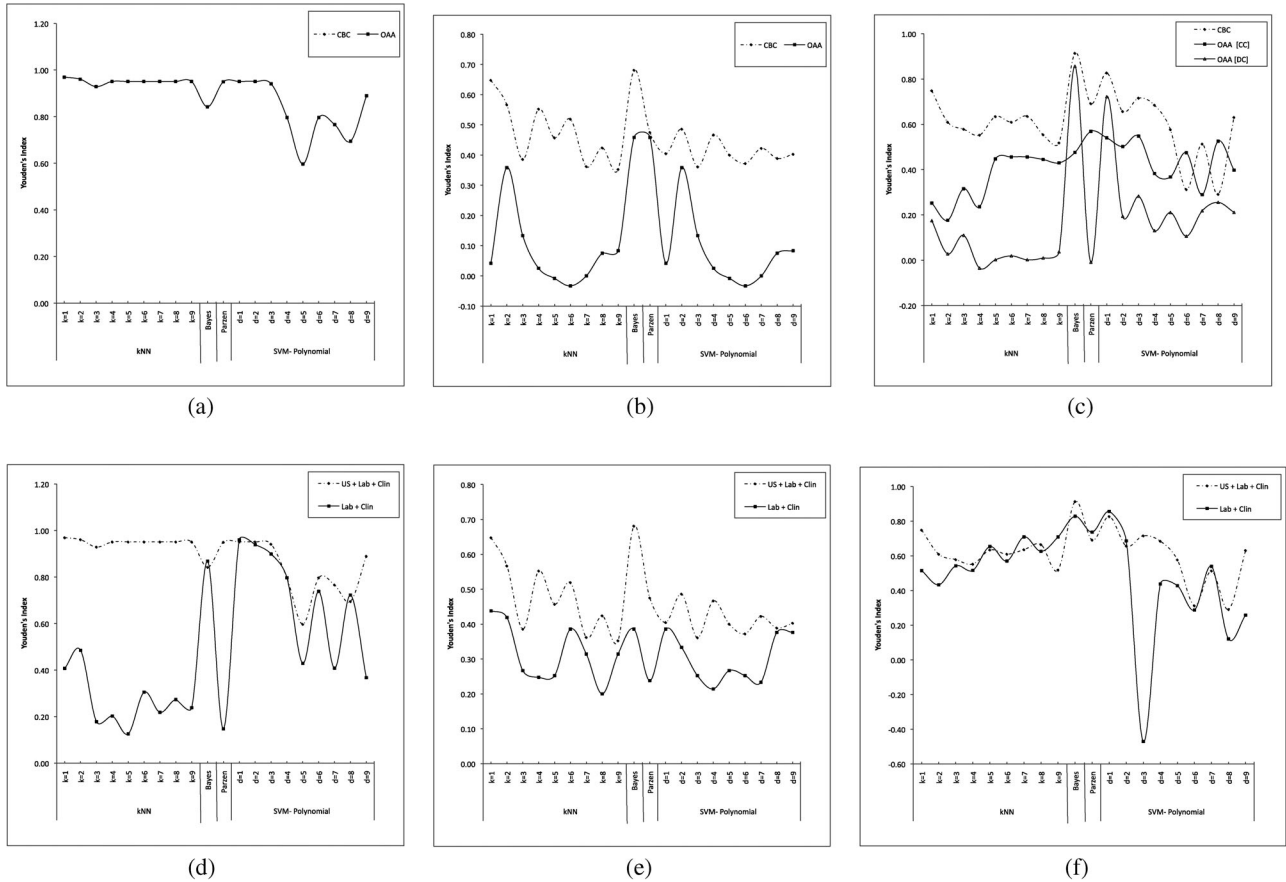


Fig. 4. Youden's index comparison results between CBC and OAA strategy [(a) normal detector, (b) chronic hepatitis detector, and (c) cirrhosis detector]; and between the multimodal and the laboratory and clinical approach [(d) normal detector, (e) chronic hepatitis detector, and (f) cirrhosis detector].

Fig. 4(a). The best result is achieved with the kNN,  $k = 1$ , and the SVM,  $d = 1$ . For computational efficiency reasons,  $k = 1$  is adopted. With this classifier, the detection accuracy for the *Normal* class is 97.92% and 99.02% for the *pathology* liver class ( $J = 0.97$ ).

*Chronic hepatitis* detector results are summarized in Fig. 4(b). CBC exhibits the best results. A *detection rate* (DR) of 76.67% is achieved for CH class with the Bayes classifier ( $J = 0.68$ ) and a DR of 91.43% for the *cirrhosis* class.

CBC outperforms the results of OAA strategy for CS III, as shown in Fig. 4(c). For the *cirrhosis* detector, the best result is achieved with the *Bayes* classifier ( $J = 0.91$ ). The individual performances showed an accuracy rate of 94.12% and 97.22% for CC and DC class, respectively. In the OAA strategy, the best classification result is for CC ( $J = 0.57$ ) and DC ( $J = 0.86$ ) classes.

Statistical differences ( $p < 0.0001$ ) were observed between the results of CBC and OAA.

*US Features Integration in the Traditional Laboratorial and Clinical CLD Classification:* The importance of US-based features in CBC accuracy was studied by comparing the results from the multimodal feature approach (US, laboratory and clinical data) and the ones from the laboratory and clinical features.

High DRs (100%) were achieved for the *normal* class in both feature sets. The best overall result for CS I ( $J = 0.97$ )

TABLE I  
CBC BEST RESULTS WITH THE TESTED FEATURE SETS (FS): (A) MULTIMODAL AND (B) LABORATORY + CLINICAL APPROACH

CS	FS	Class	Best Performance			
			DR (%)	OA (%)	J	Classifier
I	A	Normal	97.92	98.67	0.97	kNN k=1
		Pathologic	99.02			
	B	Normal	100.00	97.30	0.96	SVM <sub>polynomial</sub> d=1
		Pathologic	96.00			
II	A	CH	76.64	87.45	0.68	Bayes
		Cirrhosis	91.43			
	B	CH	76.67	70.00	0.44	kNN k=1
		Cirrhosis	67.14			
III	A	CC	94.12	95.71	0.91	Bayes
		DC	97.22			
	B	CC	91.18	91.43	0.86	SVM <sub>polynomial</sub> d=1
		DC	94.44			

was achieved with the kNN classifier ( $k = 1$ ), as illustrated in Fig. 4(d). This result showed an OA of 98.67%, with a DR of 97.92% and of 99.02% for the *normal* class and *pathologic* class, respectively (see Table I).

The results in Fig. 4(e) and Table I show that CS II had low DR. The best classification was reported with the Bayes classifier, where the proposed multimodal approach achieved the best results ( $J = 0.68$ ). Despite these results, a closer inspection reveals that the inclusion of US-based features improved CS II. The DR of *cirrhosis* class was enhanced from 67.14% (laboratory and clinical set) to 91.43%.

TABLE II  
MEAN, STANDARD DEVIATION (SE), AND MUTUAL CORRELATION (MC) OF  
THE SELECTED FEATURES

Features	CS I					
	Normal			Pathology		
	mean	SE	MC	mean	SE	MC
$a_{0,1}$ (HH <sub>1</sub> )	-0.28	0.14	0.10	-0.16	0.19	0.37
Glycemia	120.65	48.22	0.07	122.86	61.01	0.16
LDH	419.13	207.81	0.10	284.07	268.77	0.35
Disease Cause	0.06	0.23	0.05	2.65	1.87	0.19
Ascites	0.07	0.26	0.12	0.32	0.47	0.31

Features	CS II					
	CH			Cirrhosis		
	mean	SE	MC	mean	SE	MC
$a_{0,1}$ (US <sub>image</sub> )	0.86	0.08	0.34	0.85	0.07	0.20
$a_{0,1}$ (LH <sub>1</sub> )	0.06	0.23	0.36	-0.09	0.20	0.17
$a_{1,0}$ (HL <sub>2</sub> )	0.10	0.09	0.19	0.07	0.07	0.14
$a_{1,0}$ (LH <sub>2</sub> )	0.15	0.07	0.18	0.11	0.07	0.15
ALT	131.00	239.42	0.26	66.11	72.82	0.12
Age	52.85	16.19	0.17	61.34	12.01	0.07

Features	CS III					
	CC			DC		
	mean	SE	MC	mean	SE	MC
$a_{0,1}$ (US <sub>image</sub> )	0.88	0.07	0.37	0.81	0.06	0.21
E (HL <sub>1</sub> )	15.40	6.67	0.13	25.70	15.94	0.21
$a_{0,1}$ (LH <sub>1</sub> )	0.06	0.17	0.37	-0.22	0.13	0.23
$a_{1,1}$ (HH <sub>1</sub> )	-0.37	0.07	0.25	-0.26	0.08	0.18
$a_{0,1}$ (HL <sub>2</sub> )	0.43	0.09	0.34	0.37	0.12	0.19
INR	1.20	0.62	0.26	1.44	0.31	0.24
Bilirubin	1.59	1.98	0.18	3.54	4.66	0.15
Ascites	0.06	0.24	0.17	0.74	0.44	0.13
GI Bleeding	0.06	0.24	0.29	0.49	0.51	0.12
Alcoholic habits	0.12	0.33	0.13	0.57	0.50	0.17

In CS III, the multimodal approach predominantly achieved the best results, as displayed in Fig. 4(f). The best performance (see Table I) was designed with the *Bayes* classifier, attaining an OA of 95.71%, with a DR of 94.12% and 97.22% for CC and DC, respectively.

In CS I and II, significant differences ( $p < 0.01$ ) were observed in the results of the two feature sets. In CS III, similar OA results were attained, but when analyzing the DR of each class, CC class reveal significant differences ( $p < 0.01$ ).

*Feature Set for Each CS:* The CBC strategy enabled the identification of the most relevant features for each stage of CLD (see Table II), based on the proposed feature selection procedure.

The *Normal* detector (CSI) is characterized mainly by clinical information. The knowledge of the disease cause and the presence of ascites are determinant in this binary discrimination. Laboratory and US features reveal, based on the mean and standard deviation (SE) values, class overlap.

In CS II, the stepwise regression method selected ALT (laboratory feature), age (clinical feature) and four US features, all related to the AR coefficients computed from the WT decomposition (3) and the original US image (1).

The discrimination in CS III, regarding CC and DC, is achieved by the selection of a subset of ten features, where five are US-based textural features, two from laboratory data (INR, bilirubin), and three related to the clinical knowledge of ascites, GI bleeding, and alcoholic habits.

#### IV. DISCUSSION

The proposed CBC algorithm for CLD diagnosis and staging was tested with a database containing multimodal data from

148 patients specifically built for this project. The selection of the appropriated features, from different sources, to each classification step enables an optimization of the discriminative power of CBC

Biochemical tests are the most discriminative features to detect initial liver disease, which confirms the usual approach used in clinical practice. However, this discriminative advantage decreases in the higher stages of CLD characterization, where the significance of US features increases.

Age can be clinically relevant, since patients with CH (infected by HCV) have a slow progression to cirrhosis, if no complication is observed [45]. Results suggest that cirrhotic patients are 10 years older than patients with CH. On the contrary, ALT may lead to unclear conclusions since any type of cell injury in the liver can cause ALT elevation [3], [5].

The selected clinical and laboratory features for the cirrhosis detector (CS III) are considered important prognostic indicators, namely INR, bilirubin, and ascites [33]. These features are used to calculate the Child-Pugh and the *model for end-stage liver disease* (score), that accurately predict the outcomes of cirrhotic patients [46].

The inclusion of US features improves CBC performance. US textural features extracted from the first-order AR model coefficients and the multiscale Haar WT analysis (level 1) are particularly relevant. This result is in accordance with the results of [21], [23]–[25]. WT [21], [23], [24] and AR coefficients [25] based features have high discriminative power in the assessment of CLD stages. 2-D WT allows spatial frequency and orientation selectivity [32]. The use of AR coefficients in WT decomposition highlight the textural pattern by showing the development of thickened bands of connective tissue which is associated with architectural distortion of liver cells. In CS III, the vertical component ( $a_{0,1}$ ) of different WT decompositions is the main discriminative factor.

In general terms, CBC hierarchical approach outperforms the OAA strategy and the results improve when US features are integrated with laboratory and clinical features. It should be stressed that when CLD is detected (CS I), CBC outperforms the results reported in [21], [24], [37].

In [21], it is referred the difficulty to classify liver fibrosis stages from US images. When addressing the CH detector, authors in [21] reported an OA of 72%, with a sensitivity of 60% for CH patients (fibrosis grade III) and 88.6% for *cirrhotic* patients (fibrosis grade IV). CBC improved these results, attaining an OA of 86.00% with a detection rate of 73.33% and 91.43% for CH and *cirrhosis* class, respectively. [8] showed slightly superior performance with an OA of 87.7% for HCV patients.

Reports indicate that SAFE biopsy method achieves, in the cirrhosis detector, an OA that range from 88.7% [8] to 92.5% [13] in HCV patients. For CC class, [12] attained a detection rate of 92.7%, in an OAA scheme. Further investigation, conducted in [7], improved this result to 94%. In a wider CLD cause spectrum, CBC achieved better results with an OA of 95.71% and a DR of 94.12% for the CC class. The feature synergy created by CBC allows a detection rate in DC of 97.22%, improving the result of 82.2% reported in [4].

CBC classification process is independent of prior cut-off values and is not limited to one cause of CLD, whereas the results from the Castera and SAFE biopsy algorithms only include HCV patients. TE (Fibroscan) has shown promising results, but its usage is limited in patients with ascites [6], [48]. CBC overcomes this limitation and the integration of ascites in CS III is considered an advantage over TE method. The CBC is clearly a valuable tool for CBC detection and screening where multimodal data usually used in different approaches is integrated in a single CAD framework.

To minimize false-negative rates, steatosis and focal liver lesions, benign (hemangioma), or malignant (hepatoma or hepatocellular carcinoma), were not included in CBC. This is acceptable because it is assumed that focal lesions does not affect the parenchyma outside the lesion area and steatosis coexist with the pathologies detected by the CBC. In future studies, hepatic steatosis and, in a wider spectrum, *nonalcoholic fatty liver disorders* (NAFLD) should be considered in a hierarchical scheme in relationship with CBC.

In the clinical environment, US liver images acquisition should follow the proposed protocol to minimize the sensitivity of the method to the US scanner and ROI selection [24] parameters. The normalization procedures, as proposed in [51], can be very useful to increase the reliability of CBC.

## V. CONCLUSION

In this study, a classification and staging strategy for CLD based on the natural evolution of the disease is proposed. The method, called the *clinical based classifier*, undergoes a pipeline of binary classification stages that mimic the differential diagnosis approach used in clinical practice. Each CS is optimized with respect to the classifier and feature set. Results show that CBC outperforms the OAA strategy and other noninvasive CLD tests. The main goal of CBC is to provide a useful diagnosis tool which may reduce, but does not replace, liver biopsy.

The strength of CBC relies on the multimodal approach, which stress the concept of combining medical data sources, and on the classification strategy that takes into account the natural evolution of CLD.

Future evolutions of the method are being considered and a CAD tool is under development to be used in clinical environment.

## ACKNOWLEDGMENT

The authors would like to thank the Liver Unit and the Department of Gastroenterology and Hepatology of Hospital de Santa Maria, for the provision of the dataset.

## REFERENCES

- [1] R. Allan, K. Thoirs, and M. Phillips, "Accuracy of ultrasound to identify chronic liver disease," *World J. Gastroenterol.*, vol. 28, no. 16, pp. 3510–3520, Jul. 2010.
- [2] L. Bolondi and L. Gramantieri, "From liver cirrhosis to HCC," *Int. Emerg. Med.*, vol. 6, pp. 93–98, Oct. 2011.
- [3] A. S. Fauci, E. Braunwald, D. L. Kasper, S. L. Hauser, D. L. Longo, J. L. Jameson, and J. Loscalzo, *Harrison's Principles of Internal Medicine*, 17th ed. New York: McGraw-Hill, 2008.
- [4] S. Gaiani, L. Gramantieri, N. Venturoli, F. Piscaglia, S. Siringo, A. D'Errico, G. Zironi, W. Grigioni, and L. Bolondi, "What is the criterion for differentiating chronic hepatitis from compensated cirrhosis? a prospective study comparing ultrasonography and percutaneous liver biopsy," *J. Hepatol.*, vol. 27, no. 6, pp. 979–985, 1997.
- [5] D. Schuppan and N. Afdhal, "Liver cirrhosis," *Lancet*, vol. 371, pp. 838–851, Mar. 2008.
- [6] U. W. Denzer and S. Luth, "Non-invasive diagnosis and monitoring of liver fibrosis and cirrhosis," *Best Pract. Res. Clin. Gastroenterol.*, vol. 23, pp. 453–460, Jun. 2009.
- [7] M. Bourliere, G. Penaranda, X. Adhoute, V. Oules, and P. Castellani, "Combining non-invasive methods for assessment of liver fibrosis," *Gastroenterol. Clin. Biol.*, vol. 32, no. 6, pp. 73–79, 2008.
- [8] L. Castera, G. Sebastiani, B. L. Bail, V. de Ledinghen, P. Couzigou, and A. Alberti, "Prospective comparison of two algorithms combining non-invasive methods for staging liver fibrosis in chronic Hepatitis C," *J. Hepatol.*, vol. 52, no. 2, pp. 191–198, 2010.
- [9] E. Carey and W. Carey, "Noninvasive tests for liver disease, fibrosis, and cirrhosis: Is liver biopsy obsolete?" *Cleveland Clin. J. Med.*, vol. 77, no. 8, pp. 519–527, Aug. 2010.
- [10] P. Cales, F. Oberti, S. Michalak, I. Hubert-Fouchard, M.-C. Rousselet, A. Konate, Y. Gallois, C. Ternisien, A. Chevailler, and F. Lunel, "A novel panel of blood markers to assess the degree of liver fibrosis," *Hepatology*, vol. 42, no. 6, pp. 1373–1381, 2005.
- [11] V. Leroy, M.-N. Hilleret, N. Sturm, C. Trocme, J.-C. Renversez, P. Faure, F. Morel, and J.-P. Zarski, "Prospective comparison of six non-invasive scores for the diagnosis of liver fibrosis in chronic Hepatitis C," *J. Hepatol.*, vol. 46, no. 5, pp. 775–782, 2007.
- [12] G. Sebastiani, A. Vario, M. Guido, F. Noventa, M. Plebani, R. Pistis, A. Ferrari, and A. Alberti, "Stepwise combination algorithms of non-invasive markers to diagnose significant fibrosis in chronic Hepatitis C," *J. Hepatol.*, vol. 44, no. 4, pp. 686–693, 2006.
- [13] G. Sebastiani, P. Halfon, L. Castera, S. Pol, D. L. Thomas, A. Mangia, V. D. Marco, M. Pirisi, M. Voiculescu, M. Guido, M. Bourliere, F. Noventa, and A. Alberti, "Safe biopsy: A validated method for large-scale staging of liver fibrosis in chronic Hepatitis C," *Hepatology*, vol. 49, no. 6, pp. 1821–1827, 2009.
- [14] W. Zwiebel, "Sonographic diagnosis of diffuse liver disease," *Semin. Ultrasound CT and MRI*, vol. 16, pp. 8–15, Feb. 1995.
- [15] R. Zheng, Q. Wang, M. Lu, S. Xie, J. Ren, Z. Su, Y. Cai, and J. Yao, "Liver fibrosis in chronic viral hepatitis: An ultrasonographic study," *World J. Gastroenterol.*, vol. 9, no. 11, pp. 2484–2489, 2003.
- [16] V. Droga and D. Rubens, *Ultrasound Secrets*. Philadelphia, PA: Hanley and Belfus, 2004.
- [17] C. Wu, "Ultrasonographic evaluation of portal hypertension and liver cirrhosis," *J. Med. Ultrasound*, vol. 16, no. 3, pp. 188–193, 2008.
- [18] M. Federle, R. Jeffrey, P. Woodward, and A. Borhani, *Diagnostic Imaging: Abdomen*. Baltimore, MD: Lippincott Williams & Wilkins, 2009.
- [19] S.-S. Yang, "Alcoholic liver disease: Clinical and sonographic features," *J. Med. Ultrasound*, vol. 16, pp. 140–149, Apr. 2008.
- [20] M. Meziri, W. Pereira, A. Abdelwahab, C. Degott, and P. Laugier, "In vitro chronic hepatic disease characterization with a multiparametric ultrasonic approach," *Ultrasonics*, vol. 43, no. 5, pp. 305–313, 2005.
- [21] W. Yeh, Y. Jeng, C. Li, P. Lee, and P. Li, "Liver fibrosis grade classification with b-mode ultrasound," *Ultrasound Med. Biol.*, vol. 29, pp. 1229–1235, 2003.
- [22] W. Yeh, Y. Jeng, C. Li, P. Lee, and P. Li, "Liver steatosis classification using high-frequency ultrasound," *Ultrasound Med. Biol.*, vol. 31, no. 5, pp. 599–605, 2005.
- [23] J. Wan and S. Zhou, "Features extraction based on wavelet packet transform for B-mode ultrasound liver images," in *Proc. 3rd Int. Congr. Imag. Signal Process.*, Oct. 2010, vol. 2, pp. 949–955.
- [24] A. Mojsilovic, S. Markovic, and M. Popovic, "Characterization of visually similar diffuse diseases from B-scan liver images with the nonseparable wavelet transform," in *Proc. Int. Conf. Imag. Process.*, 1997, vol. 3, pp. 541–549.
- [25] T. Wang, J. Saniie, and X. Jin, "Analysis of low-order autoregressive models for ultrasonic grain signal characterization," *IEEE Trans. Ultrason., Ferroelectr., Frequency Control*, vol. 38, no. 2, pp. 116–124, Mar. 1991.
- [26] N. Farnoud, M. Kolios, and S. Krishnan, "Ultrasound backscatter signal characterization and classification using autoregressive modeling and machine learning algorithms," in *Proc. 25th Annu. IEEE Int. Conf. Eng. Med. Biol. Soc.*, Sep. 2003, vol. 3, pp. 2861–2864.
- [27] K. Wear, R. Wagner, and B. Garra, "Comparison of autoregressive spectral estimation algorithms and order determination methods in ultrasonic tissue

- characterization," *IEEE Trans. Ultrason., Ferroelectr., Frequency Control*, vol. 42, no. 4, pp. 709–716, Jul. 1995.
- [28] J. Girault, F. Ossant, A. Ouahabi, D. Kouame, and F. Patat, "Time-varying autoregressive spectral estimation for ultrasound attenuation in tissue characterization," *IEEE Trans. Ultrason., Ferroelectr., Frequency Control*, vol. 45, no. 3, pp. 650–659, May 1998.
- [29] D. Cavouras, I. Kandarakis, I. Theotokas, E. Kanellopoulos, D. Triantis, I. Behrakis, E. K. Manesis, I. Vafiadi-Zoumpouli, and P. Zoumpoulis, "Computer image analysis of ultrasound images for discriminating and grading liver parenchyma disease employing a hierarchical decision tree scheme and the multilayer perceptron neural network classifier," *Stud. Health Technol. Inf.*, vol. 43, pp. 522–26, 1997.
- [30] S. Nawaz and A. H. Dar, "Hepatic lesions classification by ensemble of svms using statistical features based on co-occurrence matrix," in *Proc. 4th Int. Conf. Emerg. Technol.*, Oct. 2008, vol. 2, pp. 21–26.
- [31] C. Lee, J. Choi, K. Kim, T. Seo, J. Lee, and C. Park, "Usefulness of standard deviation on the histogram of ultrasound as a quantitative value for hepatic parenchymal echo texture: Preliminary study," *Ultrasound Med. Biol.*, vol. 32, no. 12, pp. 1817–1826, 2006.
- [32] S. Theodoridis and K. Koutroumbas, *Pattern Recognition*, 4th ed. New York: Academic, 2008.
- [33] G. D'Amico, G. Garcia-Tsao, and L. Pagliaro, "Natural history and prognostic indicators of survival in cirrhosis: Systematic review of 118 studies," *J. Hepatol.*, vol. 44, no. 1, pp. 217–231, 2006.
- [34] S. Sherlock and J. Dooley, *Diseases of the liver and Biliary System*, 11th ed. Oxford, U.K.: Blackwell Science Ltd., 2002.
- [35] G. Cawley and N. Talbot, "Efficient leave-one-out cross-validation of kernel fisher discriminant classifiers," *Pattern Recog.*, vol. 36, pp. 2585–2592, 2003.
- [36] J. O. Rawlings, S. G. Pantula, and D. A. Dickey, *Applied Regression Analysis: A Research Tool*. New York: Springer-Verlag, 1998.
- [37] Y. Kadah, A. Farag, J. Zurada, A. Badawi, and A. Youssef, "Classification algorithms for quantitative tissue characterization of diffuse liver disease from ultrasound images," *IEEE Trans. Med. Imag.*, vol. 15, no. 4, pp. 466–478, Aug. 1996.
- [38] R. O. Duda, P. E. Hart, and D. G. Stork, *Pattern Classification*, 2nd ed. New York: Wiley, 2000.
- [39] R. M. Haralick, K. Shanmugam, and I. Dinstein, "Textural features for image classification," *IEEE Trans. Syst., Man, Cybern.*, vol. SMC-3, no. 6, pp. 610–621, Nov. 1973.
- [40] F. M. Valckx and J. M. Thijssen. (1997). Characterization of echographic image texture by cooccurrence matrix parameters. *Ultrasound Med. Biol.*, [Online]. 23(4), pp. 559–571, Available: <http://www.sciencedirect.com/science/article/pii/S0301562997000410>
- [41] R. Takalo, H. Hytti, and H. Ihalainen, "Tutorial on univariate autoregressive spectral analysis," *J. Clin. Monit. Comput.*, vol. 19, no. 6, pp. 401–410, Dec. 2005.
- [42] P. J. Brockwell and R. A. Davis, *Introduction to Time Series and Forecasting*, 2nd ed. New York: Springer-Verlag, Mar. 2002.
- [43] J. Bleck, U. Ranft, M. Gebel, H. Hecker, M. Westhoff-Bleck, C. Thiesemann, S. Wagner, and M. Manns, "Random field models in the textural analysis of ultrasonic images of the liver," *IEEE Trans. Med. Imag.*, vol. 15, no. 6, pp. 796–801, Dec. 1996.
- [44] A. Berzigotti, J. G. Abraldes, P. Tandon, E. Erice, R. Gilabert, and J. C. García-Pagan, J. Bosch, "Ultrasonographic evaluation of liver surface and transient elastography in clinically doubtful cirrhosis," *J. Hepatol.*, vol. 52, no. 6, pp. 846–853, 2010.
- [45] A. Sangiovanni, G. M. Prati, P. Fasani, G. Ronchi, R. Romeo, M. Manini, E. Del Ninno, A. Morabito, and M. Colombo, "The natural history of compensated cirrhosis due to Hepatitis C virus: A 17-year cohort study of 214 patients," *Hepatology*, vol. 43, no. 6, pp. 1303–1310, 2006.
- [46] E. Cholongitas, G. V. Papatheodoridis, M. Vangeli, N. Terreni, D. Patch, and A. K. Burroughs, "Systematic review: The model for end-stage liver disease: Should it replace child-pugh's classification for assessing prognosis in cirrhosis?" *Aliment. Pharmacol. Ther.*, vol. 22, no. 11–12, pp. 1079–1089, 2005.
- [47] P. Ferenci, A. Lockwood, and K. Mullen, "Hepatic encephalopathy-definition, nomenclature, diagnosis, and quantification: Final report of the working party at the 11th world congresses of gastroenterology, vienna, 1998," *Hepatology*, vol. 35, pp. 716–721, 2002.
- [48] J. O. Smith and R. K. Sterling, "Systematic review: Non-invasive methods of fibrosis analysis in chronic Hepatitis C," *Aliment. Pharmacol. Ther.*, vol. 30, no. 6, pp. 557–576, 2009.
- [49] V. Kaul, F. Friedenberg, and L. Braitman, "Development and validation of a model to diagnose cirrhosis in patients with Hepatitis C," *Amer. J. Gastroenterol.*, vol. 97, pp. 2623–2628, 2002.
- [50] R. Duin, P. Juszczak, P. Paclik, E. Pkalska, D. de Ridder, D. Tax, and S. Verzakov. (2007). PR-tools4.1, a matlab toolbox for pattern recognition. [Online]. Available: <http://prtools.org>
- [51] J. Thijssen, A. Starke, G. Weijers, A. Haudum, K. Herzog, P. Wohlsein, J. Rehage, and C. De Korte, "Computer-aided B-mode ultrasound diagnosis of hepatic steatosis: A feasibility study," *IEEE Trans. Ultrason., Ferroelectr., Frequency Control*, vol. 55, no. 6, pp. 1343–1354, Jun. 2008.



**Ricardo T. Ribeiro** received the B.Sc. degree in radiology from the Lisbon School of Health Technology, Polytechnic Institute of Lisbon, Lisbon, Portugal, and the M.Sc. degree from the University of Evora, Evora, Portugal. He is currently working toward the Ph.D. degree in biomedical engineering at the Institute for Systems and Robotics, Instituto Superior Técnico, the Technical University of Lisbon in collaboration with the University of Lisbon Medical School.

He is currently an Adjunct Professor at Lisbon School of Health Technology. His current research interests include the use of machine learning, computer vision, and tissue characterization for the classification of ultrasound imaging. He is also engaged in clinical research in ultrasound imaging.



**Rui Tato Marinho** received the M.D. degree from the Faculty of Medical Sciences, New University of Lisbon, Lisbon, Portugal, and the Ph.D. degree from the Faculty of Medicine, University of Lisbon.

He is currently the Gastroenterologist and Hepatologist at the Medical School of Lisbon, Hospital Santa Maria, Lisbon, Portugal.

Dr. Marinho is the Editor-in-Chief of *Acta Médica Portuguesa*, and the Scientific Journal of Portuguese Medical Association (*Ordem dos Médicos*). He is also an Adviser of the Viral Hepatitis Prevention Board

and the President of the Portuguese College of Hepatology of the Portuguese Medical Association.



**J. Miguel Sanches** (SM'11) received the E.E., M.Sc., and Ph.D. degrees from the Instituto Superior Técnico (IST), Technical University of Lisbon, Lisbon, Portugal, in 1991, 1996, and 2003, respectively.

He is currently a Professor with the Department of Bioengineering, Instituto Superior Técnico and the Researcher at the Institute for Systems and Robotics, Technical University of Lisbon. His work has been focused on Biomedical Engineering, namely, in Biomedical Signal and Image Processing, and Physiological Modeling of Biological Systems.

Dr. Sanches is a senior member of the IEEE Engineering in Medicine and Biology Society and a member of the Bio Imaging and Signal Processing Technical Committee of the IEEE Signal Processing Society and the president of the Portuguese Association of Pattern Recognition, affiliated to the International Association of Pattern Recognition.